Dynamics of Nitric Oxide Controlled by Protein Complex in Bacterial System

Erina Terasaka[a,b], Kenta Yamada[c], Po-Hung Wang[c], Kanta Hosokawa[a,b], Raika Yamagiwa[a,b], Kimi Matsumoto[a,b], Shoko Ishii[a,b], Takaharu Mori[c], Kiyoshi Yagi[c], Hitomi Sawai[a,b], Hiroyuki Arai[d], Hiroshi Sugimoto[a], Yuji Sugita[c,e,f,g], Yoshitsugu Shiro[a,b,1] and Takehiko Tosha[a,1]

[a]Biometal Science Laboratory, RIKEN SPring-8 Center, Kouto, Sayo, Hyogo 679-5148, Japan, [b]Graduate School of Life Science, University of Hyogo, Hyogo 678-1297, Japan, [c]RIKEN Theoretical Molecular Science Laboratory, Wako, Saitama 351-0198, Japan, [d]Department of Biotechnology, Graduate School of Agricultural and Life Sciences, University of Tokyo, Tokyo 113-8657, Japan, [e]RIKEN, iTHES, Wako, Saitama 351-0198, Japan, [f]RIKEN Advanced Institute for Computational Science, Kobe, Hyogo 650-0047, Japan, [g]RIKEN Quantitative Biology Center, Kobe, Hyogo 650-0047, Japan

[1]**To whom correspondence should be addressed**: Yoshitsugu Shiro or Takehiko Tosha, RIKEN SPring-8 Center, Kouto, Sayo, Hyogo 679-5148, Japan, Tel.: +81-791-58-2817; E-mail: yshiro@sci.u-hyogo.ac.jp (Y.Shiro) or ttosha@spring8.or.jp (T.T.)

Supporting Information

SI Materials and Methods

Modeling of the *cd*$_1$NiR:cNOR complex for MD simulation. The plasma membrane of *P. aeruginosa* was mimicked by preparing a mixture of POPE (3-palmitoyl-2-oleoyl-D-glycero-1-phosphatidylethanolamine), POPG (3-palmitoyl-2-oleoyl-D-glycero-1-phosphatidylglycerol), and PVCL2 (1,1'-palmitoyl-2,2'-vacenoyl cardiolipin) at a ratio POPE:POPG:PVCL2 = 70:15:15 using CHARMM-GUI Membrane Builder (1) and equilibrated for 1.75 ns using NAMD (2). The orientation of the *cd*$_1$NiR:cNOR complex was estimated from that of cNOR in the OPM database (3) and was energy-minimized using the HDGB implicit membrane model (4). The missing residues of NorB (M1-K9 and R459-A465), NorC (M1-T4), and *cd*$_1$NiR (K1-K5) were modeled using CHARMM (5). Cavities in the *cd*$_1$NiR:cNOR complex were filled with water molecules by using the DOWSER program (6). The protonation states of the titratable residues in the *cd*$_1$NiR:cNOR complex were determined according to the pK_a values predicted by PROPKA3.1 (7). The starting structure of the MD simulation was solvated and neutralized with 150 mM NaCl solution. The initial box size was 150 × 150 × 160 Å^3. The CHARMM C36 parameters for proteins and the lipid bilayer were used, while the missing parameters for heme *c* and d_1 were derived from the CHARMM C27 parameters. The non-heme iron(II) is not available in the CHARMM C27 parameters and therefore we utilized Won's parameter (8) for non-heme Fe$_B$(II) in the active site of cNOR.

MD simulation of the *cd*$_1$NiR:cNOR complex. Temperature and pressure were maintained with the Langevin thermostat and barostat. Long-range electrostatic interactions were computed with the Particle Mesh Ewald method (9, 10) with a grid space of about 1.0 Å, and Lennard-Jones interactions were truncated at a cutoff of 12 Å using a force switching function (11). All bonds involving H atoms were treated as rigid using the RATTLE and SETTLE methods (12, 13). A time step of 2 fs was employed for the integration with the velocity-Verlet algorithm. To equilibrate the simulation system, we added positional restraints of 1.0 kcal·mol^{-1}·Å^{-2} to the heavy atoms of the protein complex, the membrane, and the water molecules observed in the crystal structure and gradually reduced the positional restraints forces. After the 24.8 ns equilibration, we conducted two 210 ns production runs, each of which started with different velocities from the Maxwell-Boltzmann distribution, in the NPT ensemble at 300 K and 1 atm without any restraints. For the analysis of hydrogen-bonding interactions, coordinates were stored at every 10 ps. Except for the first step in the equilibration (using NAMD), the GENESIS package (14) was used for the MD simulation.

NO diffusion simulation between *cd*$_1$NiR and cNOR. To examine NO diffusion in the *cd*$_1$NiR:cNOR complex, we carried out another MD simulations including explicit NO molecules in the system. The initial structure for the simulations was taken from the MD snapshot at 20 ns of the trajectory 1 of the 210 ns production run without NO molecules. The heavy-atom r.m.s. deviation for the protein complex of the initial structure with respect to the crystal structure was 2.0 Å. All force field parameters for proteins, lipids, water molecules, and ions were the same as the parameters used in our simulation without NO molecules. The parameter for NO was adapted from a 3-site

fixed-charged molecular model (15, 16) that has two atomic sites at the nitrogen and oxygen atoms and a virtual site at the center of geometry. All three sites carry charges so as to reproduce the experimental dipole and quadrupole moments of the isolated NO molecule. Lennard-Jones parameters were only assigned to the atomic sites.

In total, 20 replicas of the *cd*$_1$NiR-NO-cNOR system were modeled: 10 replicas with two NO molecules, each at the active site pocket of *cd*$_1$NiR, and 10 replicas with four NO molecules, with two more NO molecules placed at protein cavities close to the active sites. Each system was simulated for 100 ns in the NPT ensemble at 300 K (Nosé-Hoover thermostat (17-19)) and 1 atm (Parrinello-Rahman barostat (20)) using GROMACS 5.1.2 (21). The initial velocity of each replica was taken from the Maxwell-Boltzmann distribution. Long-range interactions were treated using the same methods and cut-offs as in the simulation of the *cd*$_1$NiR:cNOR complex without NO. All bonds involving H atoms were treated as rigid using the LINCS method (22). From the 20 trajectories (30 NO trails from the active site of *cd*$_1$NiR monomer that interacts with cNOR) 20 events of NO escaping from *cd*$_1$NiR were observed. In 13 cases of these 20 events, the migration of NO into the hydrophobic core of the membrane was observed within 30 ns. The average time the escaped NO molecules stayed in water was only 21.4 ns. Eventually, in 4 cases, NO entered the active site cavity in cNOR during the simulation (100 ns) (Fig. 5*A* and *SI Appendix*, Fig. S7 *A*-*C*) and the average time of these 4 NO molecules stayed in the membrane before entering the active site cavity of cNOR was 23.4 ns.

To get insights into driving force of NO diffusing from the membrane into cNOR, we calculated the (hydrophobic) void volume in the membrane and cNOR. We defined a (rectangular) box in the simulation system containing only cNOR and membrane (Fig. S8*A*). All other components (i.e. water molecules, counter-ions, NO molecules, and *cd*$_1$NiR) were not included in this analysis. The size of this box is 149.226 × 149.226 × 42.215 Å^3. The x- and y- dimensions are the same as those for the simulation box while the z-dimension is the membrane thickness, as defined by the average distance between phosphorous atoms in the upper and lower leaflet. Then we calculated the available void volume inside the box using a spherical probe with an effective radius of NO molecule (2.11 Å) as shown in Fig. S8. We randomly tried to insert the probe into the box and accept the attempt only if the minimum distance between the probe and any atom is larger than the sum of the probe and the van der Waals radius. The available volume is estimated from the number of successful inserted spheres (23).

In Fig. S8*B*, we define V^S, the total void volume in the box using all the atoms. Next, the same calculation is applied to all the lipid atoms for getting V^P, which is the summation of protein volume and cavity volume for protein and membrane (Fig. S8*C*). The void volume for membrane, V^M, is estimated from a pure membrane system as shown in Fig. S8*D*-*F*. We applied this procedure for MD snapshots of the *cd*$_1$NiR:cNOR complex and membrane systems.

With the calculated available volume, we can obtain the fraction of the available volume for membrane and cNOR, $P^A_{membrane}$ and P^A_{cNOR}, respectively, by following equations:

$$P^A_{membrane} = V^M/V^B$$

$$P^{A}_{cNOR} = (V^{S} - rV^{M})/ (V^{P} - rV^{M})$$
$$r = N_{L}{}^{S}/N_{L}{}^{M}$$

where V^{B} and r are the volume of the membrane system (Fig. S8*E*) and membrane size ratio between membrane system and the original system (as defined by the number of lipids in the membrane system, $N_{L}{}^{M}$, and the original system, $N_{L}{}^{S}$), respectively. The calculated $P^{A}_{membrane}$ and P^{A}_{cNOR} were 0.023% and 0.66%, respectively.

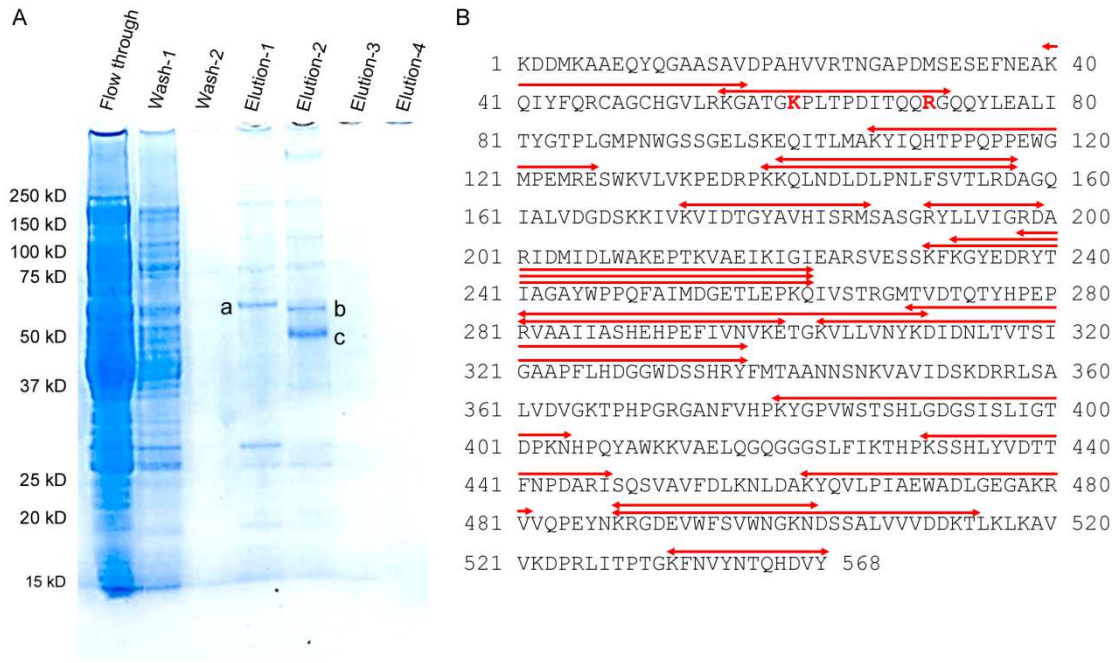

Fig. S1. Exploring the interaction proteins for cNOR using a pull-down assay. (*A*) Analysis of possible binding partners of cNOR by SDS-PAGE. Cys86 of the NorB subunit of cNOR, the only free cysteine residue in cNOR, was biotinylated using a Biotin Labeling Kit – SH (Dojindo). Biotinylated cNOR was loaded onto a streptavidin column to immobilize cNOR through biotin-streptavidin interactions, then the soluble fraction from anaerobically cultured *P. aeruginosa* was loaded onto the cNOR-immobilized column. After the column was washed with 20 mM HEPES buffer pH 7.0 containing 0.1% DTM, bound proteins were eluted by step-wise increases in NaCl concentration (10, 50, 100 and 500 mM for elution 1, 2, 3 and 4, respectively). The protein bands detected in the SDS-PAGE gel (samples a, b and c) were analyzed using the peptide mass fingerprint (PMF) method. The PMF results suggested that samples a, b and c contained GroEL (56 kDa), *cd*$_1$NiR (60 kDa for monomer) and serine protease (50 kDa), respectively, while the PMF method identified the number of peptides arising from *cd*$_1$NiR in all samples a-c. (*B*) The peptides identified by the PMF method for sample b. Red arrows above the amino acid sequence of *cd*$_1$NiR indicate the peptides identified by the PMF method. The identified peptide includes the residues in the cNOR binding site (*bold red* letter).

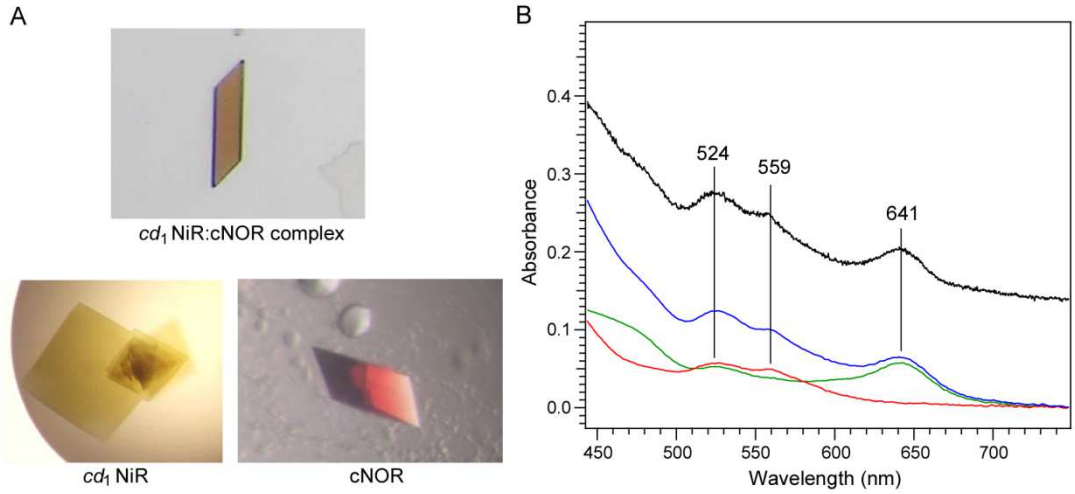

Fig. S2. (*A*) A single crystal obtained from a mixture of cNOR and *cd*$_1$NiR. The crystals of cNOR and *cd*$_1$NiR are also shown for comparison. (*B*) Optical absorption spectra of the single crystal of the *cd*$_1$NiR:cNOR complex and solution samples. Spectra shown are from the crystalline sample of the *cd*$_1$NiR:cNOR complex (black), the solution sample of cNOR (red), the solution sample of *cd*$_1$NiR (green) and the solution mixture of cNOR and *cd*$_1$NiR (blue). The molar ratio of the *cd*$_1$NiR dimer:NorBC complex is 1:2 and thus this molar ratio corresponds to the ratio of the two enzymes in the crystallized complex. The spectrum of the crystalline sample was obtained using a homemade system at 100K. All solution spectra were recorded on a U-3010 spectrophotometer (Hitachi) at ambient temperature. The samples were dissolved in 20 mM HEPES buffer pH 7.0, 150 mM NaCl containing 0.1% (w/v) DTM. The spectrum of the *cd*$_1$NiR:cNOR complex is almost identical to that of the solution mixture of *cd*$_1$NiR and cNOR.

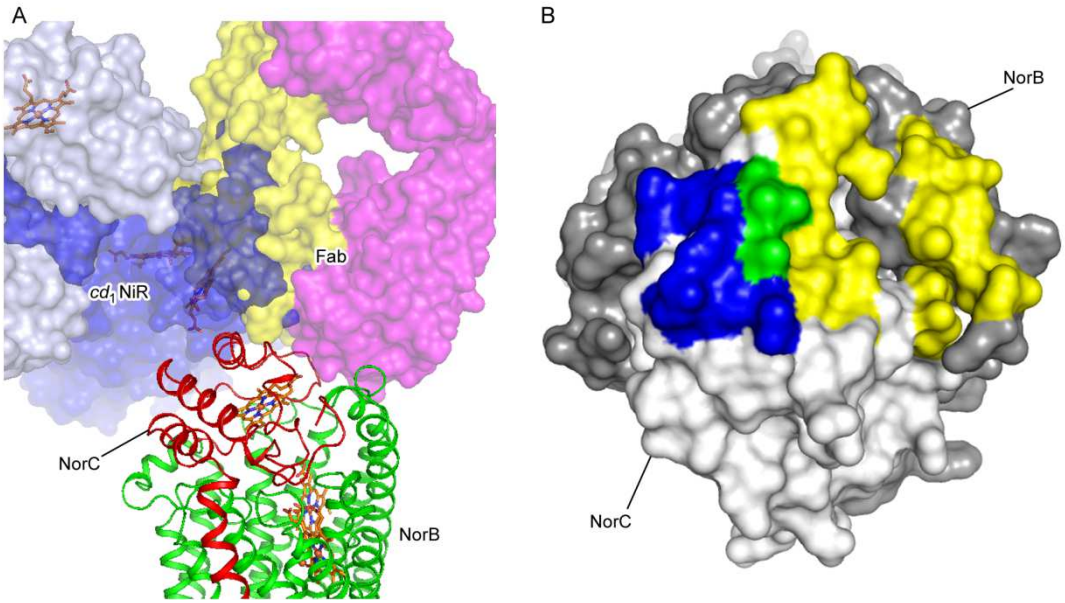

Fig. S3. Comparison of the *cd*$_1$NiR binding site with that of Fab in cNOR. (*A*) Superposition of the *cd*$_1$NiR:cNOR complex and the Fab:cNOR complex. Green and red ribbons represent NorB and NorC respectively. *cd*$_1$NiR bound to cNOR are shown by blue surface. Light and heavy chains of Fab bound to cNOR are shown by yellow and magenta surfaces, respectively. (*B*) Mapping of the *cd*$_1$NiR and Fab binding sites on cNOR viewed from periplasmic side. Blue, yellow and green surfaces represent the *cd*$_1$NiR binding site, Fab binding site and overlapping area of *cd*$_1$NiR and Fab binding sites, respectively.

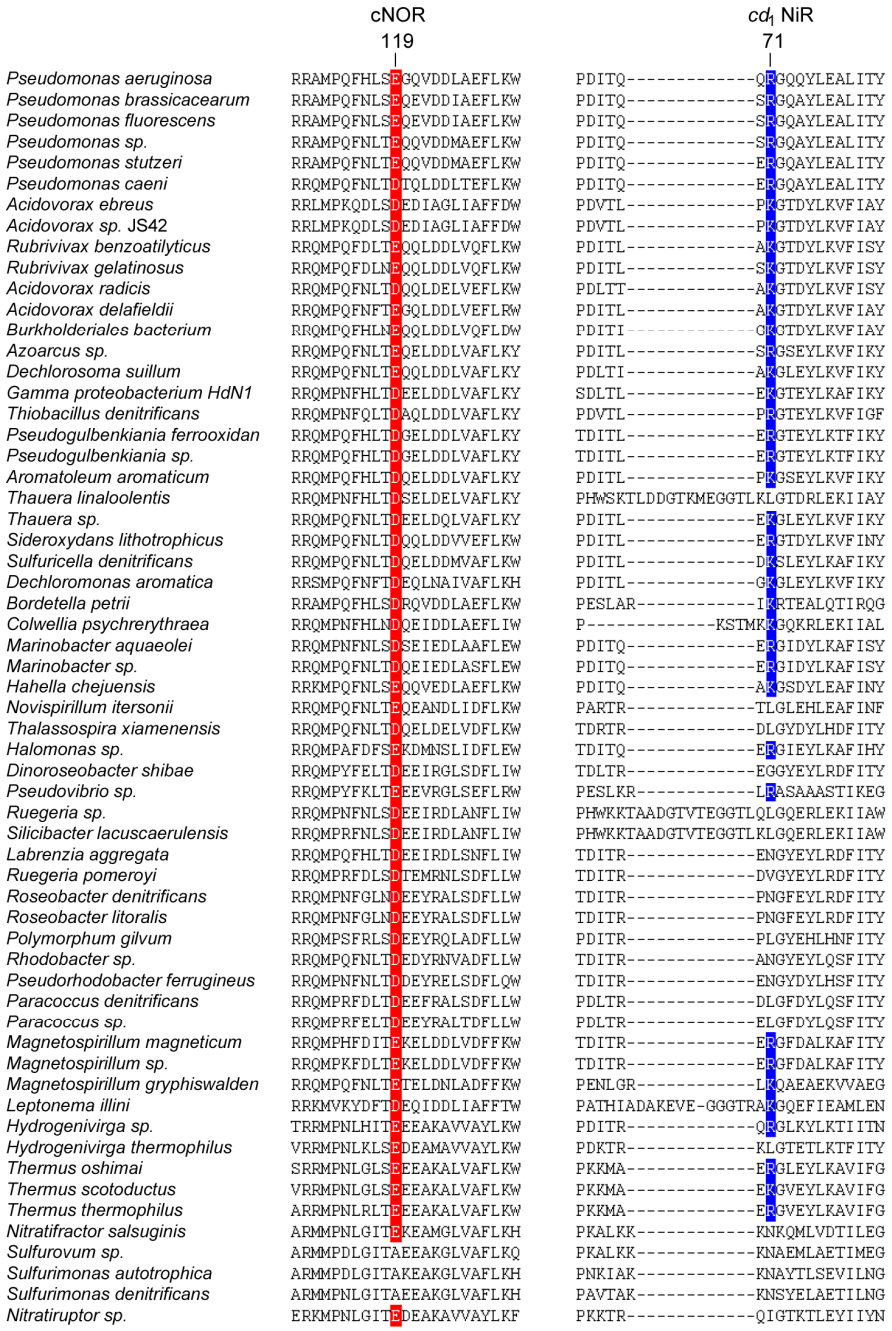

Fig. S4. Sequence alignments of the amino acid residues involved in the salt bridge formation in the *cd*$_1$NiR:cNOR complex. The sequences for the alignments were from organisms expressing both cNOR and *cd*$_1$NiR. The sequences were aligned using ClustalX. Negatively charged residues at position 119 in the NorC subunit of cNOR and positively charged residues at position 71 in *cd*$_1$NiR are highlighted with red and blue, respectively.

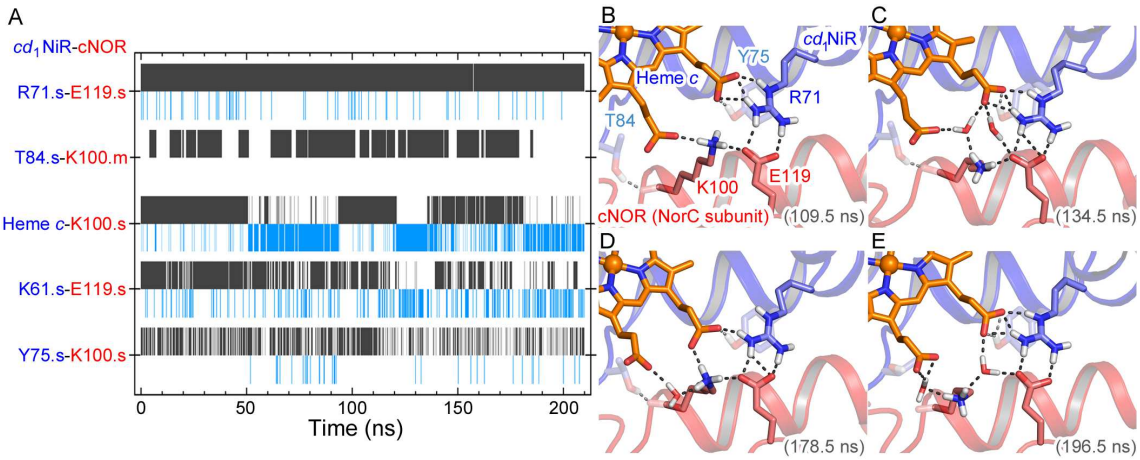

Fig. S5. (*A*) Fluctuations in interenzyme hydrogen-bonding interactions in the *cd*$_1$NiR:cNOR complex during MD simulation (see *SI Appendix*, Movie S2). The formations of direct hydrogen-bonds and water-mediated interactions, which were extracted from MD trajectory 1, are represented by black and cyan lines, respectively. Pairs of frequently interacting residues are represented by blue and red for *cd*$_1$NiR and cNOR, respectively. The letters ‘s’ or ‘m’ after the residues indicate side-chain or backbone, respectively, for the interacting atoms. The criteria for judging the formation of a hydrogen bonding interaction is an N(O)–O length < 3.5 Å and an N(O)–H–O angle > 90°. (*B*, *C*, *D* and *E*) Typical snapshots of the *cd*$_1$NiR:cNOR interface at 109.5, 134.5, 178.5 and 196.5 ns in trajectory 1, respectively. Dashed lines represent hydrogen-bonding interactions and salt bridge. Residues that frequently formed hydrogen-bonds are shown as sticks.

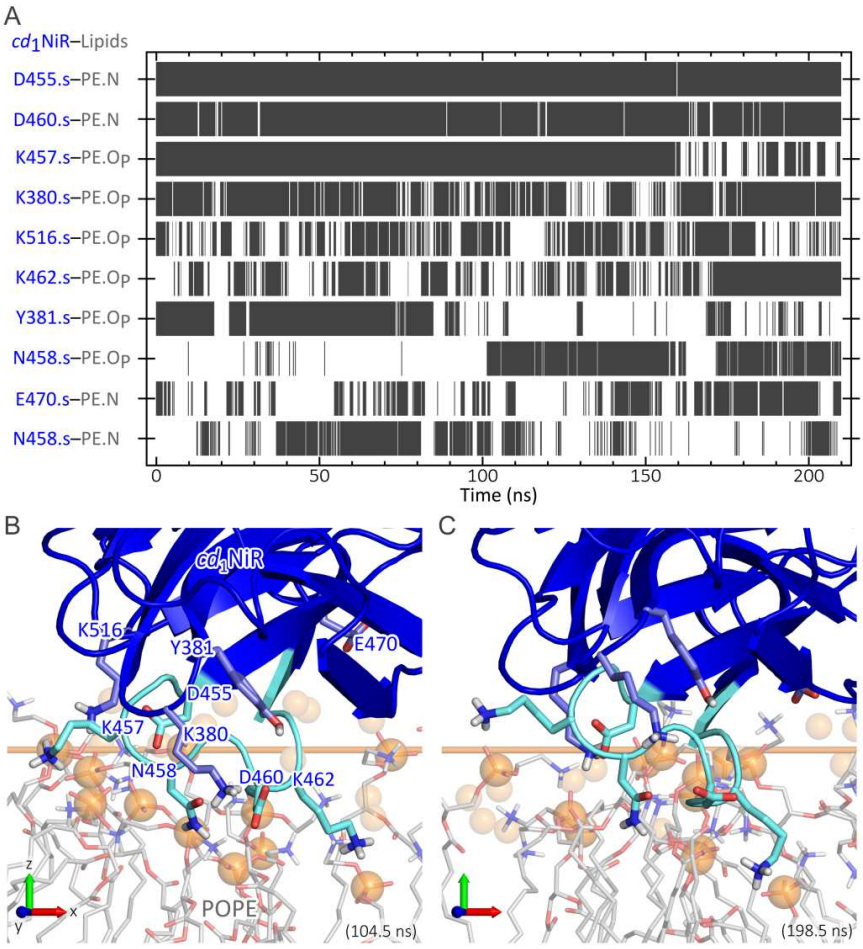

Fig. S6. Fluctuations in hydrogen-bonding interactions between *cd*1NiR and the model membrane during MD simulation. (*A*) Dynamics of the hydrogen-bonding interactions between *cd*1NiR and the model membrane (a mixture of POPE, POPG and PVCL2) over the simulation time. The formations of hydrogen-bonds between *cd*1NiR and lipid molecule, which were extracted from trajectory 1, are represented by black lines. Frequently interacting residues of *cd*1NiR are represented in blue and 's' means side-chain for the interacting atom. Although the model membrane consists of POPE, POPG and PVCL2, the POPE molecules formed hydrogen-bonds with *cd*1NiR much more frequently than the other lipid molecules. PE, N and O_P represent POPE, amine nitrogen and phosphate oxygen atoms, respectively, as the interaction sites. Hydrogen bonding interactions were judged using the same criteria as described in Fig. S5. (*B* and *C*) Typical snapshots of the *cd*1NiR–model membrane interface at 104.5 and 198.5 ns in trajectory 1, respectively. Orange spheres denote the phosphorous atoms of POPE molecules. A thick orange line denotes the average z position of the phosphorous atoms of the upper leaflet in each snapshot.

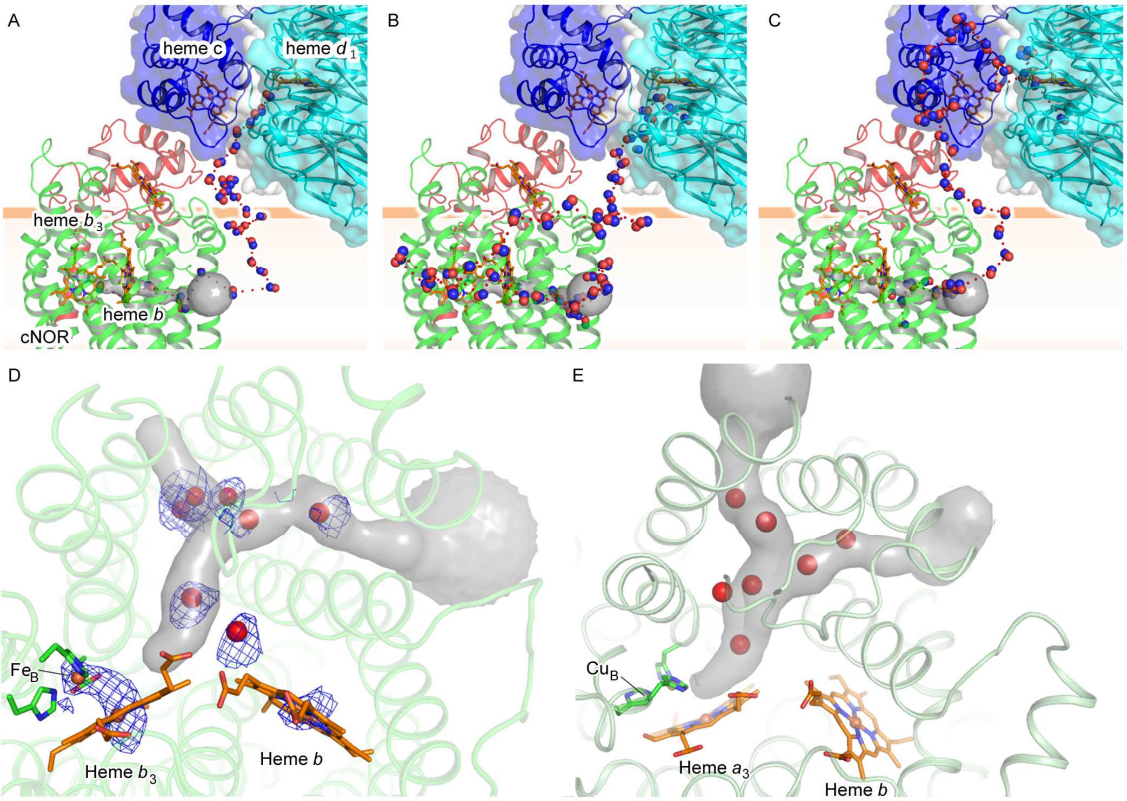

Fig. S7. Possible NO transfer pathway(s) in the *cd*$_1$NiR:cNOR complex. (*A*, *B* and *C*) NO trails obtained by the selected MD simulations. The NO trails are represented by red dotted curve, and some NO molecules on the trail are represented by red (oxygen atom) and blue (nitrogen atom) balls. The NO molecule produced at the d_1 active center of *cd*$_1$NiR escaped through a cavity located at the interface of the d_1 (blue surface) and *c* (cyan surface) domains of *cd*$_1$NiR in *A* and *B*, whereas, in *C*, the NO molecule escaped the other pathway. However, in any cases shown here, the NO molecule rapidly migrates into the biological membrane and reaches the active center of cNOR through a hydrophobic NO binding channel, as shown in Fig. 5*A*. (*D*) Potential NO transfer pathway in cNOR deduced from the xenon binding sites. Possible NO transfer channel in cNOR, viewed from the periplasmic side, is shown with xenon atoms. The NO transfer channel in cNOR predicted from CAVER analysis is shown by a gray surface. The xenon atoms are shown as red spheres. Blue mesh represents anomalous map contoured at the 2σ level. The heme cofactors are shown by orange sticks. The xenon atoms track a continuous Y-shaped channel which leads from the protein surface to the active center of cNOR. (*E*) Well-defined O_2 transfer channel in cytochrome *c* oxidase with xenon atoms.

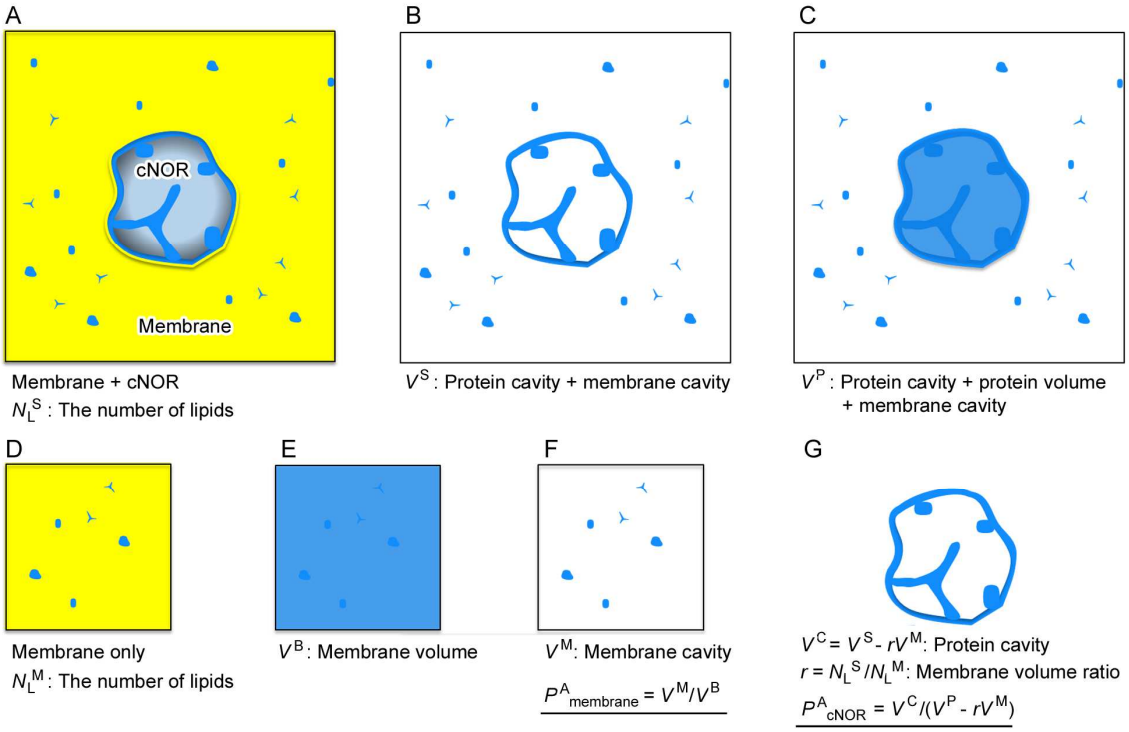

Fig. S8. Estimation method for available volume (cavity) for hydrophobic NO molecule in the biological membrane and cNOR. (*A*) Schematic view of the simulation system. The light gray object and the yellow region represent cNOR and the biological membrane, respectively. The blue regions are the voids that are available to a spherical probe. This system contains N_L^S lipids. (*B*) Definition of V^S. The V^S value is total volume of the protein cavity and the membrane cavity which are shown by blue. (*C*) Definition of V^P. The V^P value is the volume occupied by protein atoms and the available volumes inside protein and membrane (all blue regions). (*D*) Schematic view of the system containing only membrane lipids. This system contains N_L^M lipids. (*E*) Definition of V^B. The V^B value is total volume of the membrane only system which includes the membrane cavity. (*F*) Definition of V^M and the fraction of available volume for membrane ($P^A_{membrane}$). The V^M value is the volume of the membrane cavity in the system shown in panel (*D*). The $P^A_{membrane}$ value is defined as V^M/V^B. (*G*) Definition of the fraction of available volume for cNOR (P^A_{cNOR}). The volume of the protein cavity (V^C) is obtained by an equation; $V^C = V^S - rV^M$, where r represents the ratio of the number of lipids in the system shown in panels (*A*) and (*D*) (N_L^S/N_L^M). The P^A_{cNOR} value is defined as $V^C/(V^P - rV^M)$.

Table S1. Data collection and refinement statistics.

	cd_1NiR:cNOR complex	Xenon derivative of cNOR
Data collection		
Wavelength (Å)	1.0	1.0
Resolution (Å) *	50-3.2 (3.31-3.20)	40-3.3 (3.36-3.30)
Space group	$P2_1$	$P2_12_12_1$
Cell dimensions		
a, *b*, *c* (Å)	111.87, 128.61, 127.81	89.84, 105.38, 192.58
α, β, γ(º)	90.00, 106.83, 90.00	90.00, 90.00, 90.00
Observed reflections	199,694	122,197
Unique reflections	56,669	27,449
R_{merge} *,†	0.117 (0.647)	0.131 (0.456)
$CC_{1/2}$ ‡	(0.659)	(0.808)
Completeness (%)*	98.7 (98.2)	98.3 (100.0)
Redundancy *	3.5 (3.3)	4.5 (4.3)
I/sigma(*I*) *	10.4 (1.9)	10.1 (3.0)
Refinement		
R_{work} / R_{free} §	0.201/0.254	0.209/0.268
No. atoms		
Protein	17,806	8,061
Ligand/ion	547	204
Water	28	0
Mean *B*-factors (Å^2)		
Protein	67.8	71.1
Ligand/ion	53.4	84.9
Water	33.0	-
R.m.s. deviation		
Bond length (Å)	0.010	0.011
Bond angles (°)	1.55	1.63
DPI (Å) ‖	0.52	0.49
Ramachandran plot ¶		
Favored region (%)	94.5	93.6
Outlier region (%)	0.3	0.8

*Values in parenthesis are for the highest resolution shell.

† $R_{merge} = \Sigma_{hkl}\Sigma_i|I_i(hkl) - \langle I(hkl)\rangle| / \Sigma_{hkl}\Sigma_i I_i(hkl)$, where $\langle I(hkl)\rangle$ is the average intensity of *i* observations.

‡ Pearson's correlation coefficient between average intensities of random half data sets for each unique reflection.

§ $R_{work} = \Sigma_{hkl}|F_{obs}(hkl) - F_{calc}(hkl)|/\Sigma_{hkl}F_{obs}(hkl)$, where F_{obs} and F_{calc} are the observed and calculated structure factors, respectively. R_{free} was calculated with 5% of the reflections.

‖ Diffraction-data precision indicator (DPI) was calculated using Sfcheck.

¶ Ramachandran plot analysis was obtained using Rampage.

Table S2. Interacting residues in the *cd*$_1$NiR:cNOR complex.

cNOR*	*cd*$_1$NiR*	Distance (Å)[†]	Formation probability in MD[‡]	
			Trajectory 1	Trajectory 2
		Van der Waals contacts[§]		
T93 sc Cγ2	R71 bb O	3.2, 3.5	-	
T93 bb O	Y75 sc Cδ2	3.4, 3.6	-	
Q96 sc Cγ	R71 sc Nη1	4.3, 3.9	-	
A97 sc Cβ	Y75 sc Cε2	3.5, 3.4	-	
K100 sc Nζ	R71 sc Nη2	3.9, 4.1	-	
K100 sc Cε	Y75 sc Oη	3.6, 3.8	-	
K100 bb O	T84 sc Cβ	3.1, 3.1	-	
K100 bb O	P85 sc Cδ	3.4, 3.5	-	
I101 sc Cγ2	G83 bb O	3.6, 3.8	-	
Q102 bb O	P85 sc Cδ	3.7, 3.6	-	
Q114 sc Cδ	L86 sc Cδ1	4.6, 3.9	-	
Q114 sc Nε2	P85 sc Cγ	3.8, 3.8	-	
H116 sc Cε1	L86 sc Cδ2	3.8, 3.4	-	
E119 sc Oε2	K61 sc Cδ	3.4, 4.0	-	
		Salt bridge		
E119 sc Oε1	R71 sc Nη2	2.5, 2.7	1.00 (0.07)	1.00 (0.06)
		Hydrogen bonds		
K100 sc Nζ	Heme *c*[‖]	4.3, 4.1	0.63 (0.53)	0.37 (0.75)
K100 sc Nζ	Y75 sc Oη	4.1, 4.1	0.57 (0.02)	0.49 (0.02)
K100 bb O	T84 sc Oγ1	4.3, 4.2	0.65 (0.00)	0.17 (0.00)
E119 sc Oε	K61 sc Nζ	4.1, 4.4	0.62 (0.24)	0.50 (0.32)

*Sc and bb indicate side-chain and backbone, respectively.

[†] Values are from the *cd*$_1$NiR1−cNOR1 and the *cd*$_1$NiR2−cNOR2 interfaces (See Fig. 1*A*).

[‡] Criteria for the formations of hydrogen bonding interactions and salt bridges during MD simulation were an acceptor-donor distance < 3.5 Å and an acceptor-H-donor angle > 90°. The formation probabilities of hydrogen-bonding interactions and salt bridge were estimated as [number of MD snapshots showing formation of the interaction]/[total number of MD snapshots (21,000)]. Values in parentheses represent the formation probability of water-mediated hydrogen-bonding interactions.

[§] Distances less than 4.0 Å are listed as van der Waals contacts.

[‖] The propionate group of heme *c*.

Supporting references

1. Wu EL, *et al.* (2014) CHARMM-GUI membrane builder toward realistic biological membrane simulations. *J Comput Chem* 35(27):1997-2004.
2. Phillips JC, *et al.* (2005) Scalable molecular dynamics with NAMD. *J Comput Chem* 26(16):1781-1802.
3. Lomize MA, Lomize AL, Pogozheva ID, & Mosberg HI (2006) OPM: orientations of proteins in membranes database. *Bioinformatics* 22(5):623-625.
4. Tanizaki S & Feig M (2006) Molecular dynamics simulations of large integral membrane proteins with an implicit membrane model. *J Phys Chem B* 110(1):548-556.
5. Brooks BR, *et al.* (2009) CHARMM: the biomolecular simulation program. *J Comput Chem* 30(10):1545-1614.
6. Zhang L & Hermans J (1996) Hydrophilicity of cavities in proteins. *Proteins* 24(4):433-438.
7. Olsson MHM, Sondergaard CR, Rostkowski M, & Jensen JH (2011) PROPKA3: consistent treatment of internal and surface residues in empirical pK_a predictions. *J Chem Theory Comput* 7(2):525-537.
8. Won Y (2012) Force field for monovalent, divalent, and trivalent cations developed under the solvent boundary potential. *J Phys Chem A* 116(47):11763-11767.
9. Darden T, York D, & Pedersen L (1993) Particle mesh Ewald - an *N*.Log(*N*) method for Ewald sums in large systems. *J Chem Phys* 98(12):10089-10092.
10. Essmann U, *et al.* (1995) A smooth particle mesh Ewald method. *J Chem Phys* 103(19):8577-8593.
11. Steinbach PJ & Brooks BR (1994) New spherical-cutoff methods for long-range forces in macromolecular simulation. *J Comput Chem* 15(7):667-683.
12. Andersen HC (1983) Rattle - a velocity version of the shake algorithm for molecular-dynamics calculations. *J Comput Phys* 52(1):24-34.
13. Miyamoto S & Kollman PA (1992) Settle - an analytical version of the shake and rattle algorithm for rigid water models. *J Comput Chem* 13(8):952-962.
14. Jung J, *et al.* (2015) GENESIS: a hybrid-parallel and multi-scale molecular dynamics simulator with enhanced sampling algorithms for biomolecular and cellular simulations. *Wiley Interdiscip Rev Comput Mol Sci* 5(4):310-323.
15. Meuwly M, Becker OM, Stote R, & Karplus M (2002) NO rebinding to myoglobin: a reactive molecular dynamics study. *Biophys Chem* 98(1-2):183-207.

16. Mishra S & Meuwly M (2009) Nitric oxide dynamics in truncated hemoglobin: docking sites, migration pathways, and vibrational spectroscopy from molecular dynamics simulations. *Biophys J* 96(6):2105-2118.
17. Nose S (1984) A unified formulation of the constant temperature molecular dynamics methods. *J Chem Phys* 81:511-519.
18. Nose S (1984) A molecular-dynamics method for simulations in the canonical ensemble. *Mol Phys* 52(2):255-268.
19. Hoover WG (1985) Canonical dynamics: Equilibrium phase-space distributions. *Phys Rev A Gen Phys* 31(3):1695-1697.
20. Parrinello M & Rahman A (1981) Polymorphic transitions in single-crystals - a new molecular-dynamics method. *J Appl Phys* 52(12):7182-7190.
21. Van Der Spoel D, *et al.* (2005) GROMACS: fast, flexible, and free. *J Comput Chem* 26(16):1701-1718.
22. Hess B, Bekker H, Berendsen HJC, & Fraaije JGEM (1997) LINCS: A linear constraint solver for molecular simulations. *J Comput Chem* 18(12):1463-1472.
23. Lourenço TC, Coelho MFC, Ramalho TC, van der Spoel D, & Costa LT (2013) Insights on the solubility of CO_2 in 1-Ethyl-3-methylimidazolium Bis(trifluoromethylsulfonyl)imide from the microscopic point of view. *Environ Sci Technol* 47(13):7421-7429.